Applied Physics Letters

Photovoltaic sensing of a memristor based in LSMO/BTO/ITO ferroionic tunnel junctions

Cite as: Appl. Phys. Lett. **120**, 034101 (2022); https://doi.org/10.1063/5.0071748
Submitted: 16 September 2021 • Accepted: 03 January 2022 • Published Online: 18 January 2022

Isabel Tenreiro, Víctor Rouco, Gabriel Sánchez-Santolino, et al.

Applied Physics Letters ARTICLE scitation.org/journal/apl

Photovoltaic sensing of a memristor based in LSMO/BTO/ITO ferroionic tunnel junctions

Cite as: Appl. Phys. Lett. **120**, 034101 (2022); doi: 10.1063/5.0071748
Submitted: 16 September 2021 · Accepted: 3 January 2022 ·
Published Online: 18 January 2022

Isabel Tenreiro,[1] Víctor Rouco,[1] Gabriel Sánchez-Santolino,[1] Fernando Gallego,[2] Carlos Leon,[1] Alberto Rivera-Calzada,[1,a)] Ivan K. Schuller,[3] and Jacobo Santamaria[1]

AFFILIATIONS

[1]Departamento de Física de Materiales, Universidad Complutense de Madrid, 28040 Madrid, Spain
[2]Unité Mixte de Physique, CNRS, Thales, Université Paris Sud, Université Paris-Saclay, F-91767 Palaiseau, France
[3]Department of Physics, Center for Advanced Nanoscience, University of California, San Diego, California 92093, USA

Note: This paper is part of the APL Special Collection on Neuromorphic Computing: From Quantum Materials to Emergent Connectivity.
[a)]**Author to whom correspondence should be addressed:** alberto.rivera@ucm.es

ABSTRACT

Memristors based on oxide tunnel junctions are promising candidates for energy efficient neuromorphic computing. However, the low power sensing of the nonvolatile resistive state is an important challenge. We report the optically induced sensing of the resistive state of a memristor based on a $La_{0.7}Sr_{0.3}MnO_3/BaTiO_3/In_2O_3{:}SnO_2$ (90:10) heterostructure with a 3 nm thick $BaTiO_3$ ferroelectric barrier. The nonvolatile memristive response originates from the modulation of an interfacial Schottky barrier at the $La_{0.7}Sr_{0.3}MnO_3/BaTiO_3$ interface, yielding robust intermediate memristive states. The Schottky barrier produces a photovoltaic response when illuminated with a 3.3 eV UV LED, which depends on the state. The open circuit voltage V_{oc} correlates linearly with the resistance of each state, enabling active sensing of the memristive state at light power densities as low as 20 mW/cm^2 and temperatures up to 100 K. This opens up avenues for the efficient and minimally invasive readout of the memory states in hybrid devices.

The development of novel material platforms for bioinspired computing is becoming an important challenge for materials science. The rapid growth of digital data has prompted the need for energy efficient computing architectures with processing capabilities far beyond the current traditional von-Neumann paradigm.[1–3] The human brain is one of the most efficient computing systems with a power consumption below 20 W.[4] Its computing elements, the neurons, are interconnected by means of synapses forming a neural network with integrated processing and memory, drastically reducing the energy fingerprint.[4–7]

Memristors are key elements for the implementation of neuromorphic computing architectures.[2–4,8–10] They display different nonvolatile resistance states depending on their electrical history, enabling artificial synapses with high storage density.[11,12] The efficient readout of these memristive states is one of the most important aspects for the implementation of memristor devices in large arrays. The individual electrical resistance readout (current measurement after applying a voltage to each device or vice versa) has a high energy cost due to the large number of memristors present in a neural network (10^{11} in the human brain). The possible implementation of memristors with optical accessibility that allows the hybrid and active electrical detection of the state with light pulses facilitates the simultaneous readout of all the devices, drastically reducing the energy cost.[13,14]

Memristors based on oxide tunnel junctions exhibit large electrical resistance ratios and the possibility to sensitively (and reproducibly) readout memory states using their nonlinear current-voltage characteristics. A wide category of memristors exploits the domain states of a ferroelectric tunnel barrier to define the intermediate resistance states.[8,9,11,15] Others rely on the sensitivity of the interfacial resistance to the oxygen stoichiometry, which can be modified with an externally applied electric field. In this case, a similar memristive response is obtained because a continuous modulation of the oxygen vacancies concentration yields intermediate memristive states.[16–22]

We have recently shown in $La_{0.7}Sr_{0.3}MnO_3$ (LSMO)/$BaTiO_3$ (BTO) ferroionic tunnel junctions that the ferroelectric polarization charges of BTO are compensated by ionized oxygen vacancies allowing for strong ionization levels and gradual buildup of an interfacial Schottky barrier giving rise to large amplitude resistive switching and memristive response.[23] Very recently, we reported photovoltaic effects of a bipolar memory based on LSMO/BTO/$In_2O_3{:}SnO_2$ (90:10) (ITO) junctions and showed that this originates at the BTO/LSMO Schottky

barrier.[24] We anticipate that the photovoltaic effect can be finely modulated by controlling the height of the Schottky barrier. This result might be of particular interest in view of the great interest attracted by photovoltaic effects of structures involving ferroelectric layers, which may be of pure ferroelectric origin or may originate at Schottky barriers at the interfaces.[13,14,20,24–29]

The present work shows the nonvolatile, optical, and active sensing of the resistance states of a memristor throughout the available resistive switching (RS) range. Ferroionic tunnel junctions (FITJs) with a LSMO (16 nm)/BTO (3 nm)/ITO (150 nm) layer structure display a robust memristive response driven by the accumulation of oxygen vacancies at the LSMO/BTO interface. The accumulation of oxygen vacancies controls the buildup of a Schottky barrier yielding the observed photovoltaic effect, which is modulated by the barrier height. Under UV irradiation, we find a linear correlation between the open circuit voltage V_{oc} and the resistance states of the device, enabling the hybrid optical-electrical sensing of the memresistance.

We fabricated oxide junctions based on the epitaxial deposition of LSMO and BTO bilayers onto (100) $SrTiO_3$ (STO) substrates using high purity oxygen (3.2 mbar) RF sputtering at 900 °C.[30,31] Figure 1(a) shows an atomic resolution high angle annular dark field (HAADF) scanning transmission electron microscopy (STEM) image of an LSMO/BTO bilayer capped with a Ni layer. Atomic resolution images demonstrate flat layers with very high-quality epitaxy. Atomic resolution compositional electron energy-loss spectroscopy (EELS) maps acquired in the green region in Fig. 1(a) reveal an atomically sharp interface between LSMO and BTO films, confirming the high quality of the heterostructure. Specimens for scanning transmission electron microscopy were prepared by conventional mechanical polishing and Ar ion milling. STEM–EELS observations are carried out in an aberration-corrected JEOL JEM-ARM 200cF electron microscope equipped with a cold field emission gun and a Gatan Quantum spectrometer. For spectrum imaging, the electron beam is scanned along the region of interest, and an electron energy-loss spectrum was acquired for every pixel with an acquisition time of 0.03 s/pixel. Random noise is removed from EELS data using principal-component analysis. Piezoelectric force microscopy of these samples, using both amplitude and phase contrast (not shown), displays hysteresis loops and ferroelectric domain reversal with a few volts applied to the tip (see Fig. 1 of Ref. 23).

Tunnel junctions are fabricated by optical lithography with a contact area of $5 \times 10\ \mu m^2$. A 150 ± 10 nm thick ITO electrode was deposited through an aluminum shadow mask with DC magnetron sputtering at room temperature. The top transparent ITO electrode allows optical access to the junction area. The electrical characterization was performed with a two-terminal configuration as shown in the inset in Fig. 1(b) with the bottom LSMO electrode grounded and applying bias to the top ITO electrode by means of an SMU Keithley 2614B source measure unit. The measured optical transmittance of the ITO electrode is over 80% at 3.2 eV, enabling the optical access to the BTO barrier for UV illumination. The junction was illuminated with a Thorlabs M375F2 LED with 375 nm (3.3 eV) UV wavelength light, shaped in a $1 \times 1\ mm^2$ spot and 1 mW maximum power measured at the sample position. Power densities are calculated by dividing the applied power to the spot area. The optoelectronic characterization between 10 and 350 K was implemented in a Montana closed cycle He cryostat equipped with low UV absorption optical windows.

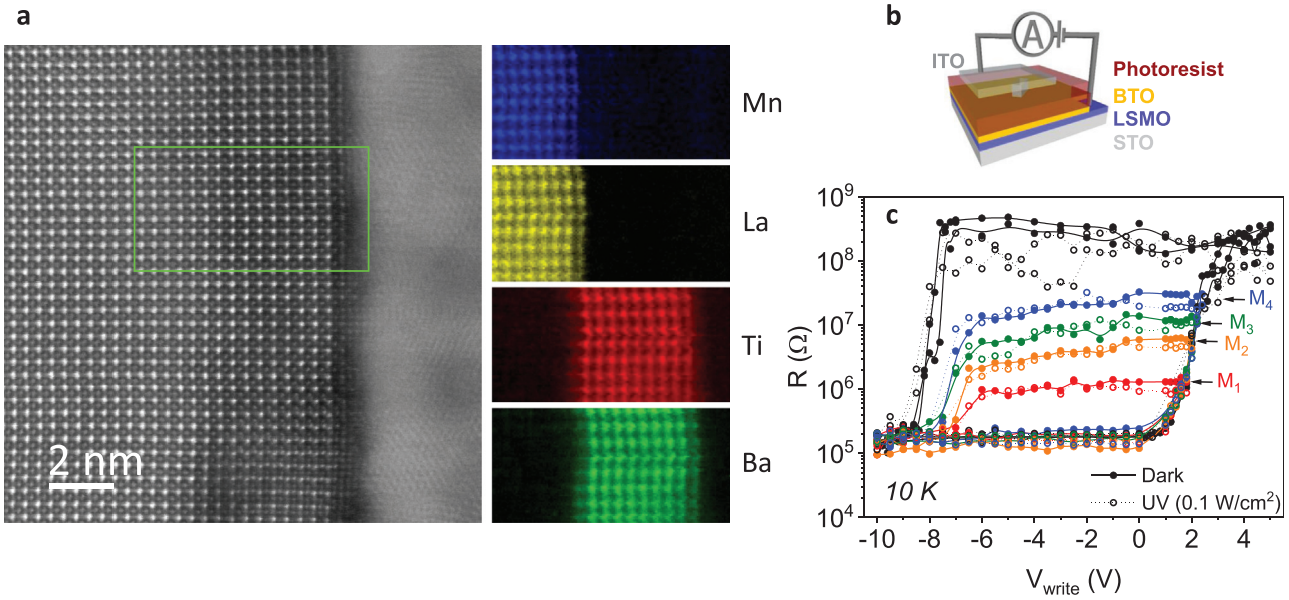

FIG. 1. (a) Atomic-resolution HAADF-STEM image obtained at an LSMO/BTO interface of a similar bilayer of 4 nm BTO thickness viewed along the [100] direction. Side panels show EELS elemental maps at the LSMO/BTO interface obtained integrating the intensities at the Mn $L_{2,3}$ (blue), La $M_{4,5}$ (yellow), Ti $L_{2,3}$ (red), and Ba $M_{4,5}$ (green) edges. (b) Sketch of the junction and the electrical connection. (c) Resistance at 10 K as a function of V_{write} in the dark (solid) and under UV (100 mW/cm^2) illumination (open). Black symbols show the major resistive switching hysteresis loop (−10 to 5 V), and colored symbols show four minor loops decreasing the maximum V_{write} in each one. The corresponding four intermediate nonvolatile memristive states are indicated with arrows.

The solid data points in Fig. 1(c) present the resistive switching loops of the FITJ appearing when cycling the voltage at 10 K in the dark. The data are obtained from the low voltage I–V as the numerical derivative dV/dI at a 100 mV reading voltage (V_{read}), after setting the resistance state with a ramp from zero to the V_{write} voltage and back to zero. Note that the two consecutive RS cycles plotted are almost indistinguishable. Black solid points in Fig. 1(c) show the main or major RS loops, where positive voltages above 4 V (electric fields directed toward the LSMO/BTO interface) saturate the high resistance state (R_{High}) or the OFF state. In this state, the I–Vs show a strongly rectifying behavior characteristic of a thermionic transport over a Schottky barrier, as shown in Fig. S1(a) of the supplementary material. The R_{High} state remains stable until negative voltages below −8.5 V are applied, when the resistance switches to the saturated low resistance state (R_{Low}) or the ON state. This switching sets on the tunneling regime, as demonstrated in Fig. S1(a) of the supplementary material, and the fits of the I–Vs to the symmetric Brinkman's tunneling model shown in the panels (b)–(d) of the same figure. The tunneling electro resistance (TER) ratio $R_{High}/R_{Low} \sim 10^4$ enables four orders of magnitude to study intermediate resistance values when minor V_{write} loops are followed. Solid colored symbols of Fig. 1(c) show four minor resistance vs V_{write} cycles in the dark, in which the voltage is only increased to $V_{write} = 1.2$–3.0 V, causing the intermediate remnant states with stable resistance (nonvolatile). In the figure, these four intermediate memristive states (M_1–M_4) are marked with arrows, showing the memristor behavior of the tunnel junction in the dark. In these samples, the increase in the resistance is reported to be a consequence of the gradual accumulation of oxygen vacancies at the bottom interface, where its presence was established from STEM EELS experiments.[23,30] The accumulation of oxygen vacancies builds up a Schottky barrier at the LSMO/BTO interface responsible of the strongly rectifying behavior of I–V s observed at large voltages [see supplementary material, Fig. S1(a)].[10,16–18] An important remark is that since both electrodes are oxide metals with similar carrier densities in the 10^{21} cm^{-3} range and, thus, similar screening lengths, a large ferroelectric electroresistance is not expected in this system.[32] The dc "write" voltage controls the accumulation of oxygen vacancies at the bottom interface, and thus, the height of the Schottky barrier allows for the stabilization of the different memristive states [Fig. 1(c)].[23] Open circles in this figure are RS loops cycling V_{write} in the same range as in the dark but under UV LED light with 100 mW/cm^2 power density. The resistance of the memristive states with light remains the same within experimental error in all the resistance range in the figure, showing that the memristive states remain stable under UV light, so that the photovoltaic response of the Schottky barrier can be used to sense the resistance of the different states without modifying them.

To analyze the maximum photovoltaic response of the FITJ, we set the high resistance state R_{High} of the device and record the I–V curves for voltages between 200 and −200 mV. This range is small enough not to change the set resistance state. Black solid points in Fig. 2(a) show the I–V curve of the FITJ at 10 K in the high resistance state, R_{High}, in the dark. The data show a forward biased diode-like behavior for negative voltages, when the electric field points from the LSMO to the BTO, according to the grounding of the LSMO layer and previous results.[23,24] The I–V characteristic (open symbols) under 3.3 eV LED radiation with 100 mW/cm^2 power density shows the photovoltaic response of the device, i.e., non-zero voltage at zero current, the open circuit voltage V_{oc}, and non-zero current at zero voltage, the short circuit current I_{sc}. Since the voltage is applied to the top electrode with the LSMO grounded, the photogenerated electrons are driven by the Schottky barrier to the top ITO electrode and the holes to the LSMO interface.[24] This produces a "positive" photocurrent and a "negative" V_{oc} in Fig. 2(a) according to the electric circuit connections specified in Fig. 1(b). In the R_{High} state, photogenerated carriers are separated by the "built-in" electric field ($\mathbf{E_{bi}}$) that arises in the depletion region of the Schottky barrier [inset of Fig. 2(a)].

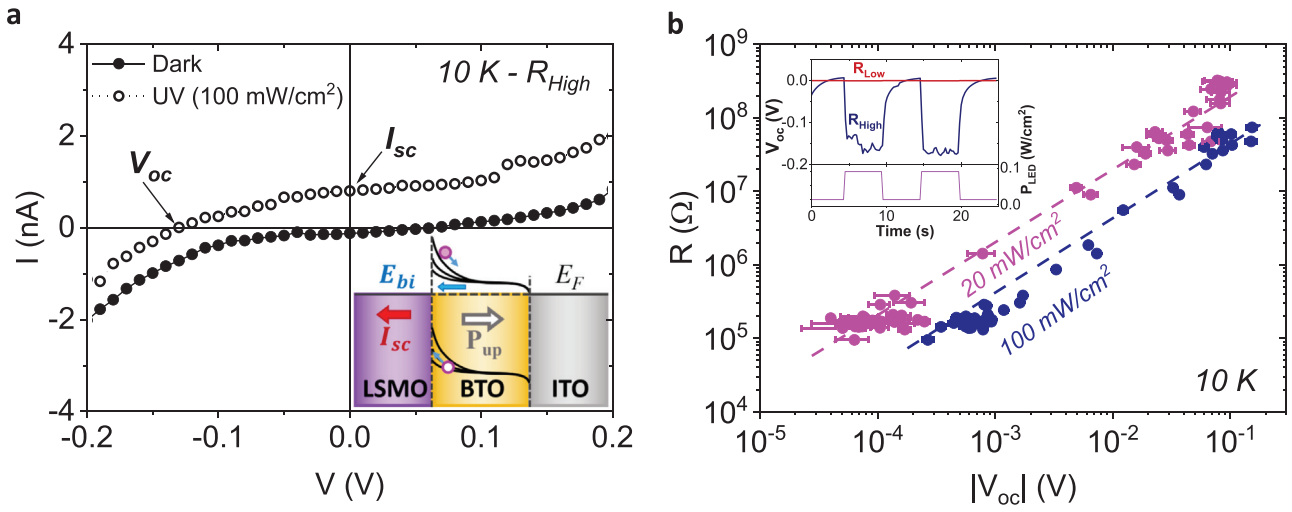

FIG. 2. (a) I–V curves in the R_{High} in the dark and under UV (100 mW/cm^2) illumination. Inset is a sketch of the band diagram, indicating the variation of the Schottky barrier for different memristive states. (b) Resistance of different memristive states at 10 K as a function of the measured $|V_{oc}|$ for 20 and 100 mW/cm^2 power densities. Dashed lines are guides for the eye with slope 1 corresponding to a linear correlation. The inset shows the V_{oc} vs time for R_{High} and R_{Low} memristive states (top curves), measured under light pulses of 5 s (bottom curve).

The carrier injection into the electrodes, holes into the LSMO, and electrons into the ITO are helped by the depolarization field that appears with the polarization pointing toward the ITO electrode.[24,29] A photocurrent (I_{sc}) is then generated in the same direction as the Schottky built in electric field $\mathbf{E_{bi}}$ and opposite to the FE polarization, as shown in the simplified band diagram in the inset of Fig. 2(a).[29]

Figure 2(b) presents the correlation of the resistance of each memristive state with the corresponding $|V_{oc}|$ observed in the same state under UV light. These data are obtained by directly measuring the active photovoltaic response V_{oc}, output by the junction without applying current, as the illumination power is turned on and off. The inset of Fig. 2(b) illustrates the time dependent voltage response of the FITJ with illumination, which defines the V_{oc} value during the 5 s light time, in the R_{High} (blue) and R_{Low} (red) states. These high sensitivity measurements allows for the detection of a residual photo response even in the low resistance state with V_{oc} values in the mV range. Considering the two sets of data of Fig. 2(b), the increase in V_{oc} with the light power density is in agreement with the Schottky transport equation[33]

$$V_{oc} = \frac{k_B T}{Nq} \ln\left(1 + \frac{I_{sc}}{I_0}\right), \tag{1}$$

with N being the ideality factor, I_{sc} being the photogenerated current, I_0 being the reversed bias saturation current, and k_BT/q being the thermal voltage. The power density enters this equation through I_{sc}, which is proportional to the light power, as shown in Fig. S2(a) of the supplementary material and in agreement with previous results.[24]

Therefore, Fig. 2(b) is the dependence of the resistance of each memristive state with the active voltage generated by the FITJ under two different power densities (100 and 20 mW/cm^2) of UV LED illumination. Within experimental error, the line with slope one in the double logarithmic plot [Fig. 2(b)] implies a linear resistance vs V_{oc} dependence. This linear behavior is explained in terms of bending of the energy bands of the FITJ barrier. An increase in the FITJ resistance implies an increase in the Schottky barrier at the LSMO/BTO interface as shown in the inset of Fig. 2(a). Furthermore, this implies an increase in the barrier built in electric field and the consequent extension of the depletion region width, so that the photogenerated carriers experience a separation with a higher electrostatic potential, showing a higher V_{oc}.

The thermionic emission current in a Schottky junction is given by[33]

$$I = AA^* T^2 \exp\left(-\frac{q\varphi_0}{k_B T}\right)\left[\exp\left(\frac{qV}{k_B T}\right) - 1\right], \tag{2}$$

where $A^* = \frac{4\pi m^* q k^2}{h^3}$ is the Richardson constant (1.2×10^6 m*/m Am^{-2} K^{-2}), m^* is the effective mass, A is the cross section of injected carriers, and φ_0 is the energy band step in the metal semiconductor interface, $\varphi_0 = \chi + (E_c - E_F)$, the semiconductor electron afinity χ plus the difference between the conduction band edge (E_c) and the Fermi level (E_F) of BTO. To calculate the open circuit voltage, the photocurrent I_{sc} is added in parallel with negative sign as it is a reversed current, and the V_{oc} can be approximated (neglecting 1 since the voltages expected are much greater than k_BT/q) as

$$V_{oc} = \frac{k_B T}{q} \ln\left(\frac{I_{sc}}{AA^* T^2}\right) + \varphi_0. \tag{3}$$

This equation explains the linear correlation of V_{oc} with the built in Schottky barrier incorporated in φ_0 at constant temperature. The linear dependence of the memristive resistance vs V_{oc} shown in Fig. 2(b) for two UV light intensities demonstrates the photovoltaic sensing of the memristive state spanning four orders of magnitude of resistance. Since the photovoltaic response is directly linked to the Schottky barrier, the linear correlation found between V_{oc} and the resistance value confirms the origin of the memristive response in the Schottky barrier generated in the minor RS cycles, in good agreement with previous results.[2,10,17,23,24]

Direct measurements of I_{sc} under illumination, without applying any voltage to the FITJ, show a constant value of approximately 1.2 nA for both the extreme R_{High} and R_{Low} memristive states, Fig. S2 of the supplementary material. The fact that I_{sc} does not depend on the memristive state resistance of the junction means that the same number of photocarriers is generated for the different states and, therefore, different Schottky barrier heights. Since BTO is the optically active layer of the FITJ under UV illumination,[24] the number of photogenerated carriers depends on the BTO bandgap, the thickness of the BTO absorbing layer, and the illuminated area of the device. None of these parameters change when the memristive state of the device is switched and the Schottky barrier modified, so the number of excitons generated when the junction is switched under UV light should remain approximately the same, as observed. The I_{sc} observed in the R_{Low} memristive state can be explained in terms of the same residual energy band bending that originates a mV photovoltaic response in the low resistance memristive state [inset to Fig. 2(b)]. This bending is enough to separate the electron-hole pairs, giving rise to the generation of a photocurrent independent of the resistance state of the junction. The linear relation of I_{sc} and the power density of the LED observed in Fig. S2(a) of the supplementary material support this scenario.[24]

Figure 3(a) shows the major RS loops at increasing temperatures, 10, 50, and 100 K. The TER ratio R_{High}/R_{Low} is reduced according to the different thermal behavior of each state. The R_{High} state has a semiconductor/insulator behavior with a resistance that decreases increasing temperature. The R_{Low} state is characterized by symmetric I–Vs that can be fitted within Brinkman's tunneling model[34] (Fig. S1 of the supplementary material) with resistance that slightly increases with temperature.[24] The weak temperature dependence of R_{Low} may be ascribed to the metallic behavior of the bottom electrode, connected in series with the junction.[35] As a result, the TER ratio is reduced, and when the intermediate memristive states are probed, the accessible window decreases.[36] Figure 3(b) presents the correlation of the resistance of the memristive states with the corresponding active voltage $|V_{oc}|$ measured, as explained in the inset of Fig. 2(b) at 10, 50, and 100 K. The same qualitative behavior is observed with increasing temperature with a linear correlation of the memristive state resistance and the voltage V_{oc} output by the FITJ. The decrease in V_{oc} observed with increasing temperature in the figure is in qualitative agreement with the temperature dependence expected from Equation 3. In a similar fashion, the I_{sc} is also decreasing with temperature as observed in Fig. S2(b) of the supplementary material, which hinders optical detection of memresistance at room temperature. Future work will be devoted to engineer FITJ with hybrid optical functionalities at room temperature. The presence of the Schottky barrier accounts *per se* for the photovoltaic effect, particularly in view of the good agreement of the open circuit voltage with the Schottky transport model.

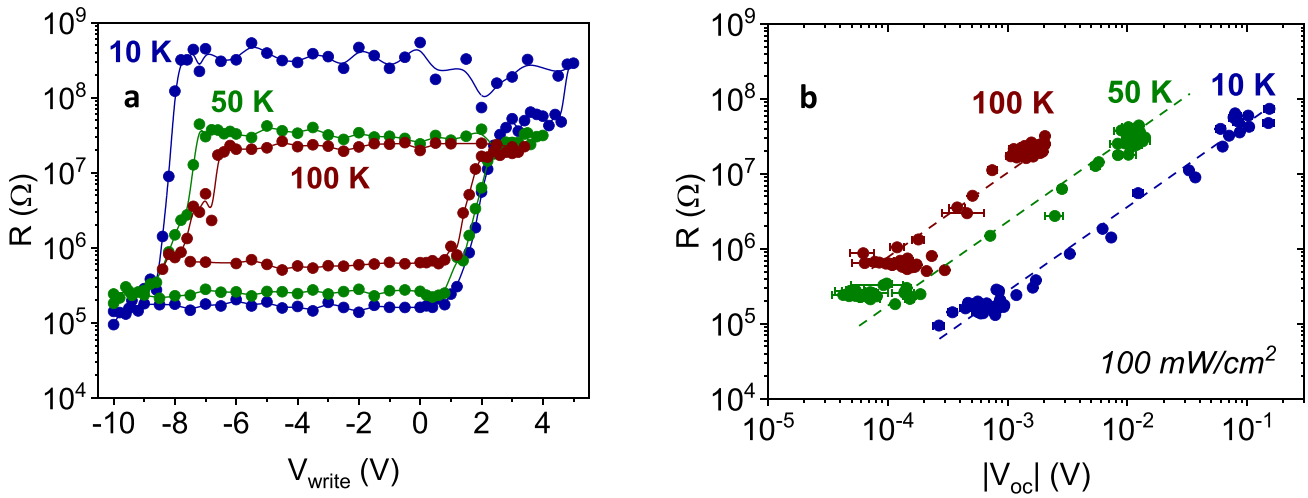

FIG. 3. (a) Resistive switching loops as a function of the temperature. (b) Resistance of the memristive states as a function of the measured $|V_{oc}|$ obtained under UV (100 mW/cm^2) illumination for 10, 50, and 100 K temperatures. Dashed lines are guide for the eye with slope 1.

Furthermore, it is important to remark that the photovoltaic effect vanishes in the low resistance state, dominated by tunneling transport. This suggests that polarization induced contributions to the photovoltaic effect[37–39] may be absent or very small for this ultrathin ferroelectric layer.

In summary, we fabricated ferroionic tunnel junctions with the LSMO (16 nm)/BTO (3 nm)/ITO (150 nm) structure that show resistive switching due to the formation of an optically active Schottky barrier at the LSMO/BTO interface. Major RS loops display maximum R_{High}/R_{Low} ratios of the order of 10^4 at 10 K, and minor cycles illustrate the existence of stable intermediate nonvolatile memristive states. Four reproducible and distinguishable states are shown to be robust under UV light, demonstrating the functionality of the FITJ device for optically induced sensing. Under UV illumination, a solid photovoltaic response appears, which is modulated by the Schottky barrier potential profile. The V_{oc} generated by the device is linearly correlated with the resistance of each memristor state, enabling optically induced sensing of the states. This important result facilitates the active and parallel sensing of memristors and other ultra-low consuming devices and opens routes for the development of both energy efficient memory and neuromorphic devices.

See the supplementary material for the transport characterization of the tunneling low resistance state and the Schottky high resistance state and the photogenerated current I_{sc} measured at different power densities and temperatures.

The transmittance characterization of the top ITO electrode was performed in collaboration with Dr. Riccardo Frisenda in the ICMM-CSIC. This work was supported by Spanish MCI through Grant Nos. MAT 2017-87134-C02 and PCI 2020-112093. G.S.-S. acknowledges financial support from Spanish MCI via Grants Nos. RTI2018-099054-J-I00 (MCI/AEI/FEDER, UE) and IJC2018-038164-I. Electron microscopy observations were carried out at the *Centro Nacional de Microscopia Electrónica*, CNME-UCM. This material was based upon the work supported by the U.S. Air Force Office of Scientific Research under Award No. FA9550-20-1-0242.

AUTHOR DECLARATIONS

Conflict of Interest

The authors have no conflicts to disclose.

DATA AVAILABILITY

The data that support the findings of this study are available from the corresponding author upon reasonable request.

REFERENCES

[1] J. Zhu, T. Zhang, Y. Yuchao, and R. Huang, Appl. Phys. Rev. **7**, 011312 (2020).
[2] R. Guo, W. Lin, X. Yan, T. Venkatesan, and J. Chen, Appl. Phys. Rev. **7**, 011304 (2020).
[3] B. Sun, G. Zhou, L. Sun, H. Zhao, Y. Chen, F. Yang, Y. Zhao, and Q. Song, Nanoscale Horiz. **6**, 939 (2021).
[4] I. Boybat, M. L. Gallo, S. R. Nandakumar, T. Moraitis, T. Parnell, T. Tuma, B. Rajendran, Y. Leblebici, A. Sebastian, and E. Eleftheriou, Nat. Commun. **9**, 2514 (2018).
[5] S. Boyn, J. Grollier, G. Lecerf, B. Xu, N. Locatelli, S. Fusil, S. Girod, C. Carrétéro, K. Garcia, S. Xavier, J. Tomas, L. Bellaiche, M. Bibes, A. Barthélémy, S. Saïghi, and V. Garcia, Nat. Commun. **8**, 14736 (2017).
[6] J. Valle, J. G. Ramírez, M. J. Rozenberg, I. K. Schuller, J. Valle, J. G. Ramírez, M. J. Rozenberg, and I. K. Schuller, J. Appl. Phys. **124**, 211101 (2018).
[7] Y. Yang, Z. Xi, Y. Dong, C. Zheng, H. Hu, X. Li, Z. Jiang, W.-C. Lu, D. Wu, and Z. Wen, ACS Appl. Mater. Interfaces **12**, 56300 (2020).
[8] D. J. Kim, H. Lu, S. Ryu, C. W. Bark, C. B. Eom, E. Y. Tsymbal, and A. Gruverman, Nano Lett. **12**, 5697 (2012).
[9] A. Chanthbouala, V. Garcia, R. O. Cherifi, K. Bouzehouane, S. Fusil, X. Moya, S. Xavier, H. Yamada, C. Deranlot, N. D. Mathur, M. Bibes, A. Barthélémy, and J. Grollier, Nat. Mater. **11**, 860 (2012).
[10] W. Lü, C. Li, L. Zheng, J. Xiao, W. Lin, Q. Li, X. R. Wang, Z. Huang, S. Zeng, K. Han, W. Zhou, K. Zeng, J. Chen, Ariando, W. Cao, and T. Venkatesan, Adv. Mater. **29**, 1606165 (2017).
[11] A. Chanthbouala, A. Crassous, V. Garcia, K. Bouzehouane, S. Fusil, X. Moya, J. Allibe, B. Dlubak, J. Grollier, S. Xavier, C. Deranlot, A. Moshar, R. Proksch, N. D. Mathur, M. Bibes, and A. Barthélémy, Nat. Nanotechnol. **7**, 101 (2012).

[12]Y. Wei, S. Matzen, G. Agnus, M. Salverda, P. Nukala, T. Maroutian, Q. Chen, J. Ye, P. Lecoeur, and B. Noheda, Phys. Rev. Appl. **12**, 031001 (2019).
[13]R. Guo, L. You, Y. Zhou, Z. Shiuh Lim, X. Zou, L. Chen, R. Ramesh, and J. Wang, Nat. Commun. **4**, 1990 (2013).
[14]W. J. Hu, Z. Wang, W. Yu, and T. Wu, Nat. Commun. **7**, 10808 (2016).
[15]V. Garcia and M. Bibes, Nat. Commun. **5**, 4289 (2014).
[16]A. Sawa, Mater. Today **11**, 28 (2008).
[17]Q. H. Qin, L. Äkäslompolo, N. Tuomisto, L. Yao, S. Majumdar, J. Vijayakumar, A. Casiraghi, S. Inkinen, B. Chen, A. Zugarramurdi, M. Puska, and S. van Dijken, Adv. Mater. **28**, 6852 (2016).
[18]Y. Yang, X. Zhang, L. Qin, Q. Zeng, X. Qiu, and R. Huang, Nat. Commun. **8**, 15173 (2017).
[19]H. Fan, C. Chen, Z. Fan, L. Zhang, Z. Tan, P. Li, Z. Huang, J. Yao, G. Tian, Q. Luo, Z. Li, X. Song, D. Chen, M. Zeng, J. Gao, X. Lu, Y. Zhao, X. Gao, and J. M. Liu, Appl. Phys. Lett. **111**, 252901 (2017).
[20]S. Gao, G. Liu, H. Yang, C. Hu, Q. Chen, G. Gong, W. Xue, X. Yi, J. Shang, and R.-W. Li, ACS Nano **13**, 2634 (2019).
[21]V. Rouco, F. Gallego, D. Hernandez-Martin, D. Sanchez-Manzano, J. Tornos, J. I. Beltran, M. Cabero, F. Cuellar, D. Arias, G. Sanchez-Santolino, F. J. Mompean, M. Garcia-Hernandez, A. Rivera-Calzada, M. Varela, M. C. Muñoz, C. Leon, Z. Sefrioui, and J. Santamaria, APL Mater. **9**, 031110 (2021).
[22]V. Rouco, R. E. Hage, A. Sander, J. Grandal, K. Seurre, X. Palermo, J. Briatico, S. Collin, J. Trastoy, K. Bouzehouane, A. I. Buzdin, G. Singh, N. Bergeal, C. Feuillet-Palma, J. Lesueur, C. Leon, M. Varela, J. Santamaría, and J. E. Villegas, Nat. Commun. **11**, 658 (2020).
[23]D. Hernandez-Martin, F. Gallego, J. Tornos, V. Rouco, J. I. Beltran, C. Munuera, D. Sanchez-Manzano, M. Cabero, F. Cuellar, D. Arias, G. Sanchez-Santolino, F. J. Mompean, M. Garcia-Hernandez, A. Rivera-Calzada, S. J. Pennycook, M. Varela, M. C. Muñoz, Z. Sefrioui, C. Leon, and J. Santamaria, Phys. Rev. Lett. **125**, 266802 (2020).
[24]A. Rivera-Calzada, F. Gallego, Y. Kalcheim, P. Salev, J. del Valle, I. Tenreiro, C. León, J. Santamaría, and I. K. Schuller, Adv. Electron. Mater. **7**, 2100069 (2021).
[25]R. Guo, L. You, W. Lin, A. Abdelsamie, X. Shu, G. Zhou, S. Chen, L. Liu, X. Yan, J. Wang, and J. Chen, Nat. Commun. **11**, 2571 (2020).
[26]C. Wang, K. Jin, Z. Xu, L. Wang, C. Ge, H. Lu, H. Guo, M. He, and G. Yang, Appl. Phys. Lett. **98**, 192901 (2011).
[27]T. Li, A. Lipatov, H. Lu, H. Lee, J.-W. Lee, E. Torun, L. Wirtz, C.-B. Eom, J. Íñiguez, A. Sinitskii, and A. Gruverman, Nat. Commun. **9**, 3344 (2018).
[28]X. Long, H. Tan, F. Sánchez, I. Fina, and J. Fontcuberta, Nat. Commun. **12**, 382 (2021).
[29]Z. Tan, L. Hong, Z. Fan, J. Tian, L. Zhang, Y. Jiang, Z. Hou, D. Chen, M. Qin, M. Zeng, J. Gao, X. Lu, G. Zhou, X. Gao, and J.-M. Liu, NPG Asia Mater. **11**, 20 (2019).
[30]G. Sanchez-Santolino, J. Tornos, D. Hernandez-Martin, J. I. Beltran, C. Munuera, M. Cabero, A. Perez-Muñoz, J. Ricote, F. Mompean, M. Garcia-Hernandez, Z. Sefrioui, C. Leon, S. J. Pennycook, M. C. Muñoz, M. Varela, and J. Santamaria, Nat. Nanotechnol. **12**, 655 (2017).
[31]J. Tornos, F. Gallego, S. Valencia, Y. H. Liu, V. Rouco, V. Lauter, R. Abrudan, C. Luo, H. Ryll, Q. Wang, D. Hernandez-Martin, G. Orfila, M. Cabero, F. Cuellar, D. Arias, F. J. Mompean, M. Garcia-Hernandez, F. Radu, T. R. Charlton, A. Rivera-Calzada, Z. Sefrioui, S. G. E. te Velthuis, C. Leon, and J. Santamaria, Phys. Rev. Lett. **122**, 037601 (2019).
[32]M. Y. Zhuravlev, R. F. Sabirianov, S. S. Jaswal, and E. Y. Tsymbal, Phys. Rev. Lett. **94**, 246802 (2005).
[33]S. M. Sze and K. K. Ng, *Physics of Semiconductor Devices (Sze—2nd Edition)* (John Wiley & Sons, 1981).
[34]W. F. Brinkman, R. C. Dynes, and J. M. Rowell, J. Appl. Phys. **41**, 1915 (1970).
[35]F. Y. Bruno, S. Boyn, S. Fusil, S. Girod, C. Carrétéro, M. Marinova, A. Gloter, S. Xavier, C. Deranlot, M. Bibes, A. Barthélémy, and V. Garcia, Adv. Electron. Mater. **2**, 1500245 (2016).
[36]D. Pantel and M. Alexe, Phys. Rev. B **82**, 134105 (2010).
[37]M. Yang, D. J. Kim, and M. Alexe, Science **360**, 904 (2018).
[38]M. Wu, Z. Jiang, X. Lou, F. Zhang, D. Song, S. Ning, M. Guo, S. J. Pennycook, J. Dai, and Z. Wen, Nano Lett. **21**, 2946 (2021).
[39]Z. Jiang, Z. Xu, Z. Xi, Y. Yang, M. Wu, Y. Li, X. Li, Q. Wang, C. Li, D. Wu, and Z. Wen, J. Mater. (published online 2021).